Geophysical Journal International

Geophys. J. Int. (2014) **197,** 1090–1095
Advance Access publication 2014 February 20

doi: 10.1093/gji/ggu037

Imaging and characterization of a subhorizontal non-welded interface from point source elastic scattering response

Shohei Minato and Ranajit Ghose

Department of Geoscience and Engineering, Delft University of Technology, the Netherlands. E-mail: s.minato-1@tudelft.nl

Accepted 2014 January 28. Received 2014 January 28; in original form 2013 November 25

SUMMARY

The inverse scattering of seismic waves can reveal the spatial distribution of the elastic compliances along a non-welded interface, such as a fracture surface. The spatial heterogeneity along the surface of a fracture is a key determinant for fracture-associated hydraulic properties. In this paper, we demonstrate that the inverse scattering solution can be successfully applied to the point source response of a subhorizontal fracture. In the scale of seismic exploration, it is more appropriate to consider spherical waves from a point source than plane waves. Further, from only the *P*-wave point source response it is possible to estimate both normal and tangential fracture compliances. The synthetic seismic wavefield due to a *P*-wave point source in a 2-D elastic medium was computed using a time-domain finite difference approach. On this spherical wave data set, the correct estimation of the position and dip of the non-welded interface was possible through reverse-time migration followed by least-square fitting of the maximum amplitude of the *P*–*P* reflection. In order to estimate the heterogeneity along the non-welded interface, we first extract the elastic wavefield at the interface position. The extrapolated wavefield is then rotated such that the horizontal axis aligns along the fracture plane. Next, using this extrapolated and rotated wavefield, we solve the linear-slip boundary condition to obtain the distribution of normal and tangential compliances. Our result shows that the estimates of normal compliance are very accurate around the dominant frequency of the incident seismic wavefield. At lower frequencies, the estimated compliance distribution is less accurate and rather smooth due to the presence of evanescent waves. Extracting the distribution of the tangential compliance requires a larger stabilization factor. For a correct estimation of the tangential compliance, one needs *S*-wave sources or multiple sources providing more grazing angles to avoid the shadow zone.

Key words: Image processing; Inverse theory; Spatial analysis; Defects; Fracture and flow; Wave scattering and diffraction.

1 INTRODUCTION

Normal and tangential compliances of a non-welded interface like a fracture, estimated from the elastic waves, are of great importance in a variety of geophysical applications. With fractures that are invisible in a given scale of seismic measurement, the fractured medium can be considered effectively anisotropic and homogeneous. The values of the compliances can then be indirectly estimated from the seismic attributes, for example, amplitude-versus-azimuth (AVAZ) distribution, normal-moveout velocity anisotropy, or shear wave splitting. For fractures with scale larger than or comparable to the seismic wavelength, the medium is heterogeneous; in that case the scattered seismic waves can be used to characterize the fractures (e.g. Willis *et al.* 2006). These large-scale fractures can have a dominant effect on the fluid flow in the subsurface.

Although spatial heterogeneity along the plane of a fracture has been ignored in most earlier studies, the fracture compliance is, in general, spatially heterogeneous (e.g. Pyrak-Nolte & Nolte 1992; Oliger *et al.* 2003; Acosta-Colon *et al.* 2009). The fracture compliance is a complex function of the roughness of the fracture surface, the distribution of contact area, the elasticity of the material filling the void at the fracture interface, and the stress field (e.g. Hudson *et al.* 1997). Therefore, the spatial distribution of the fracture compliances reflects the heterogeneous distribution of these parameters. In the case of the seismically visible large-scale fractures, the estimation of the heterogeneous compliance distribution is key to evaluating the spatially heterogeneous mechanical and hydraulic properties of the fractured medium. In the scale of the seismically invisible fractures, the heterogeneous compliance distribution affects the frequency-dependent anisotropy of the effectively

homogeneous medium (e.g. Baird *et al.* 2013). This apparent frequency dependence due to the heterogeneous distribution of fracture compliances (Pyrak-Nolte & Nolte 1992) is useful to partially explain the scaling behaviour of compliances between different scales of seismic measurements (Worthington & Lubbe 2007).

The studies related to spatial heterogeneity of fracture compliance, though undoubtedly important, are scarce. Oliger *et al.* (2003) discussed focusing effects in transmitted waves due to heterogeneous fracture compliance. Acosta-Colon *et al.* (2009) measured the heterogeneous transmission coefficients with different beam widths. Laboratory experiments have led to the estimation of reflection and transmission coefficients from measured transmitted or reflected waves (e.g. Lubbe *et al.* 2008). Since these experiments involved single-sensor measurements, it was possible to obtain only the spatially averaged reflection and transmission responses, which poses difficulty in recovering the true heterogeneous distribution. In this vein, Pyrak-Nolte & Nolte (1992) and Biwa *et al.* (2007) considered a random compliance distribution as sensed by transmitted and reflected waves, respectively.

Recently, we have developed a new approach to estimate the lateral variation in fracture compliance by solving the inverse scattering problem for the backscattered wavefield recorded with an array of receivers (Minato & Ghose 2013). The method can be applied not only to laboratory and surface seismic reflection data, but also to single borehole data to capture accurately the heterogeneity along the near-wellbore fractures for which the transmission seismic response is not available. The consideration of plane wave in this approach (Minato & Ghose 2013) is useful for application to relatively high-frequency exploration seismic data or to far-field, low-frequency data (e.g. earthquake seismograms). However, when the seismic source is located relatively close to the fracture and to the receivers—in the scale of the seismic wavelength, then the consideration of a point source and propagating spherical waves is necessary. This has been the goal of the present research. Additionally, here we have considered the dip of the fracture to be variable. We also obtain the structural parameters of the fracture, that is, position and orientation of the fracture through reverse time migration. To represent a practical situation, a *P*-wave point source has been considered. For a *P*-wave point source, the obliquely incident waves at the fracture produce converted *S* waves. This gives us the opportunity to estimate both normal and tangential compliance distributions from the recorded backscattered wavefield due to a *P*-wave source, which was previously not possible. The data is represented in the time–space domain rather than in the frequency–wavenumber domain of Minato & Ghose (2013). This clarifies the working of this approach and the importance of various wave types generated at the fracture. Note that Minato & Ghose (2014) successfully extracted the power spectral density (PSD) of the heterogeneous fracture compliance from the scattered elastic wavefield using amplitude information alone. The present approach and that of Minato & Ghose (2013) differ from it because they use the phase together with the amplitude to estimate the exact distribution of the heterogeneous compliance distribution.

In this paper, starting from the displacement–discontinuity boundary condition, we briefly explain the numerical calculation of the scattered wavefield due to a *P*-wave point source and a subhorizontal fracture embedded in a 2-D homogeneous medium. Then we illustrate our inverse scattering procedure applied to data in time–space domain and solve the problem to estimate the heterogeneous compliance distribution.

2 POINT SOURCE RESPONSE OF A SUBHORIZONTAL FRACTURE WITH SPATIALLY HETEROGENEOUS COMPLIANCE

We calculate the backscattered elastic wavefield from a single non-welded interface embedded in a 2-D homogeneous elastic medium (Fig. 1a). We consider the displacement–discontinuity boundary condition (Schoenberg 1980). This boundary condition can be used to approximate the wide scale range of a thin discontinuity due to a fracture—varying from microcracks (e.g. Baik & Thompson 1984; Hudson *et al.* 1997) to faults (e.g. Worthington & Hudson 2000). In the displacement–discontinuity model, normal and tangential compliances (η_N and η_T, respectively) define the magnitude of the displacement–discontinuity across the fracture plane due to wave-induced stress field as, $[\mathbf{u}](x) = \mathbf{Z}(x)\boldsymbol{\tau}(x)$, where $[\mathbf{u}] = ([u_x]\ [u_z])^T$ and $\boldsymbol{\tau} = (\tau_{xz}\ \tau_{zz})^T$ are, respectively, the displacement–discontinuity vector and the stress traction vector at the fracture plane. We assume the diagonal structure of the compliance matrix (Schoenberg 1980), that is, $\mathbf{Z}(x) = \mathrm{diag}[\eta_T(x), \eta_N(x)]$. Note that the x-axis is taken along the fracture plane. Therefore, for a dipping fracture, we need to rotate the data in order to apply this boundary condition.

A 2-m-long fracture, dipping 10° from the horizontal (see red line in Fig. 1a), is embedded in a homogeneous background. The centre of the fracture is 1.5 m away from a *P*-wave point source. 401 receivers are installed at a constant spacing, 0.5 m below the source, along a 4-m-long horizontal line. The geometry is realistic in the scale of material testing and of geophysical experiments in the laboratory. Rotating the horizontal axis by 90° will correspond to a single borehole seismic acquisition geometry or a vertical seismic profiling (VSP) geometry. We assume the receivers to be located below the point source for the possibility of extrapolating the source wavefield. In surface seismic measurements, generally the source and receivers are located at the same depth level. In this case, if independent estimates of source wavefield and source radiation pattern are available, the method will be directly applicable. Note that this approach works well for a longer/shorter fracture by using a lower/higher frequency. Minato & Ghose (2013) have shown that the result obtained by this approach in the laboratory scale can be upscaled to the field scale if the relative scales for the seismic wavelength, fracture length, fracture depth, correlation length of the compliance distribution and sampling interval are preserved.

A staggered-grid finite difference time domain (FDTD) approach (Coates & Schoenberg 1995) has been adopted to include the displacement–discontinuity boundary condition and model the elastic wavefield. Fig. 1(b) shows the considered heterogeneous spatial distribution of compliance ($\eta_T = \eta_N$) along the fracture. The heterogeneous compliance model has 10 per cent standard deviation from the average value of 1×10^{-14} m Pa^{-1}. The compliance value at the two edges of the fracture are tapered to zero (i.e. completely welded). The background medium parameters ($V_P = 6.3$ km s^{-1}, $V_S = 3.4$ km s^{-1}, $\rho = 3080$ kg m^{-3}) and the average compliance value are inspired by the experiment of Lubbe *et al.* (2008). We assume the normal compliance to be same as the tangential compliance ($\eta_N = \eta_T$), which is often used as an approximation for gas-filled open fractures (e.g. Sayers 2002; Willis *et al.* 2006). However, they can be different in this approach.

Fig. 2 shows for a *P*-wave point source the calculated response (horizontal and vertical components of the particle velocity) along the receiver line. Notice three clear arrivals: direct *P* wave,

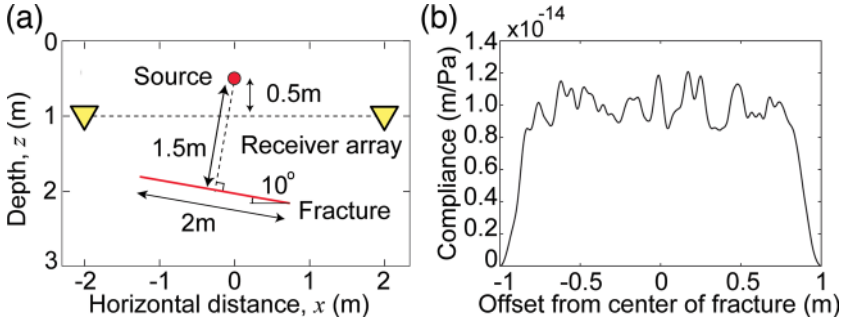

Figure 1. (a) Source and receiver geometry for the calculation of the elastic wavefield: a *P*-wave point source and a single subhorizontal fracture embedded in a homogeneous background. (b) The spatially heterogeneous distribution of elastic compliance along the fracture, used to calculate the wavefield.

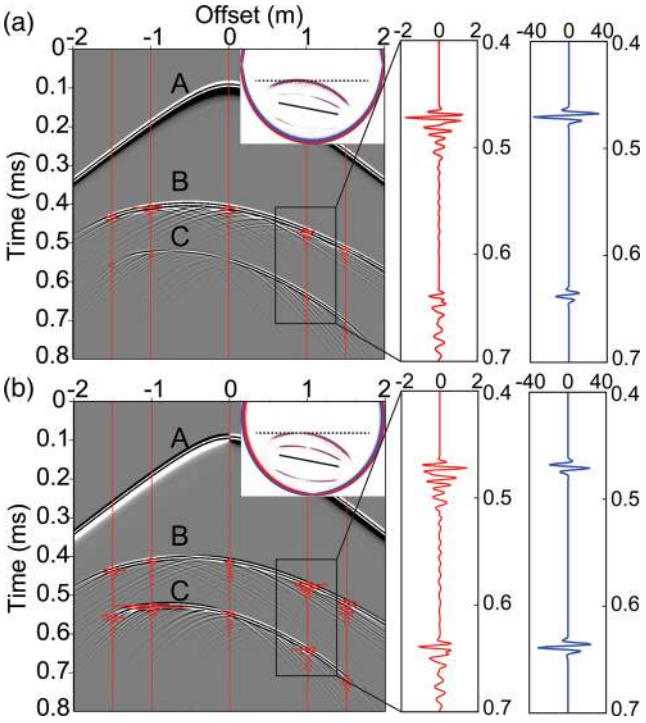

Figure 2. (a) Common source gather: calculated vertical component of the particle velocity at the receiver array due to a *P*-wave point source. The red traces show the difference in waveform between wavefields calculated using homogeneous (spatially invariant) and heterogeneous compliance distributions (Fig. 1b). The blue trace is the waveform for homogeneous compliance. A, B and C are direct *P* wave, reflected *P* wave and converted *S* wave, respectively. The inset shows a snapshot of the calculated wavefield at 0.4 ms. (b) Same as (a) but for the horizontal component of the particle velocity.

reflected *P* wave and converted *S* wave (A, B and C in Fig. 2). The large amplitudes in Fig. 2 are clipped in order to make the small diffracted arrivals visible. These non-specular diffracted waves are due to the heterogeneous compliance distribution. In order to investigate the difference in seismic response between homogeneous and heterogeneous fracture compliances, we calculate the response again but using a spatially invariant compliance distribution (blue traces in Fig. 2) and subtract it from the heterogeneous compliance wavefield at source–receiver offsets −1.5, −1, 0, 1 and 1.5 m. The value of the constant compliance is the average value of the heterogeneous compliance distribution (1×10^{-14} m Pa^{-1}). Red traces in Fig. 2 show the change due to introduction of the fracture-compliance heterogeneity; the difference is clear in the amplitude of the specular reflections and in the presence of the non-specular diffractions (coda wave) in both vertical/horizontal components. This observation is new and it provides insights toward novel fracture-characterization possibilities.

3 FRACTURE IMAGING AND CHARACTERIZATION USING BACKSCATTERED ELASTIC WAVEFIELD DUE TO A POINT SOURCE

To represent the observed data, 10 per cent white noise is added to the particle velocity data (*P*-wave common-source gather), estimated above (Fig. 2). Following Minato & Ghose (2013), we estimate compliance distribution in two steps: (1) extrapolation of the observed wavefield to the fracture depth and (2) solving the displacement–discontinuity boundary condition. Note that Minato & Ghose (2013) used incident pseudo-plane wave (Gaussian beam) and horizontal fractures. Leiderman *et al.* (2007) also considered similar conditions for a multilayered medium with an incident Gaussian beam and horizontal fractures. Here we consider spherical waves sensing a dipping fracture.

The first step consists of wavefield extrapolation using incident and backscattered wavefields followed by imaging of fracture position and inclination. The wavefield extrapolation used in Minato & Ghose (2013) is defined in the frequency–wavenumber domain as,

$$\hat{\tau}^{+}(z) = \hat{\mathbf{L}}_2^{+}\hat{\mathbf{W}}(\hat{\mathbf{L}}_2^{+})^{-1}\hat{\mathbf{v}}^{+}(z_r), \tag{1}$$

$$\hat{\tau}^{-}(z) = \hat{\mathbf{L}}_2^{-}\hat{\mathbf{W}}^{\dagger}(\hat{\mathbf{L}}_2^{-})^{-1}\hat{\mathbf{v}}^{-}(z_r), \tag{2}$$

where z_r and z are, respectively, the receiver depth and an arbitrary depth below the receiver. $\hat{\boldsymbol{\tau}}$ and $\hat{\mathbf{v}}$ are the stress vector and the particle-velocity vector, respectively. Superscripts $\pm$ indicate the downgoing and the upgoing wavefields. $\hat{\mathbf{L}}_2^{\pm}$ is a function of the medium parameters (i.e. elastic constants) and $\hat{\mathbf{W}}$ and $\hat{\mathbf{W}}^{\dagger}$ are, respectively, the forward extrapolation operator and the matched inverse operator (Wapenaar & Berkhout 1989), which contain the medium velocities and the propagation distance $|z - z_r|$. Since we know that the reflected and diffracted waves are upgoing waves and the incident wave is a downgoing wave, we extrapolate the wavefields separately.

The approach requires estimation of incident and backscattered wavefields along the fracture plane (Minato & Ghose 2013). Since our formulation (eqs 1 and 2) allows extrapolation of the wavefield at all depths below the receiver array, we first extrapolate the wavefield in depth and extract the wavefield along the known fracture position. Further, since the boundary condition is applied at the fracture plane, the axes which represent the wavefield (particle velocities and stress field) are rotated so that the horizontal axis lies in the fracture plane.

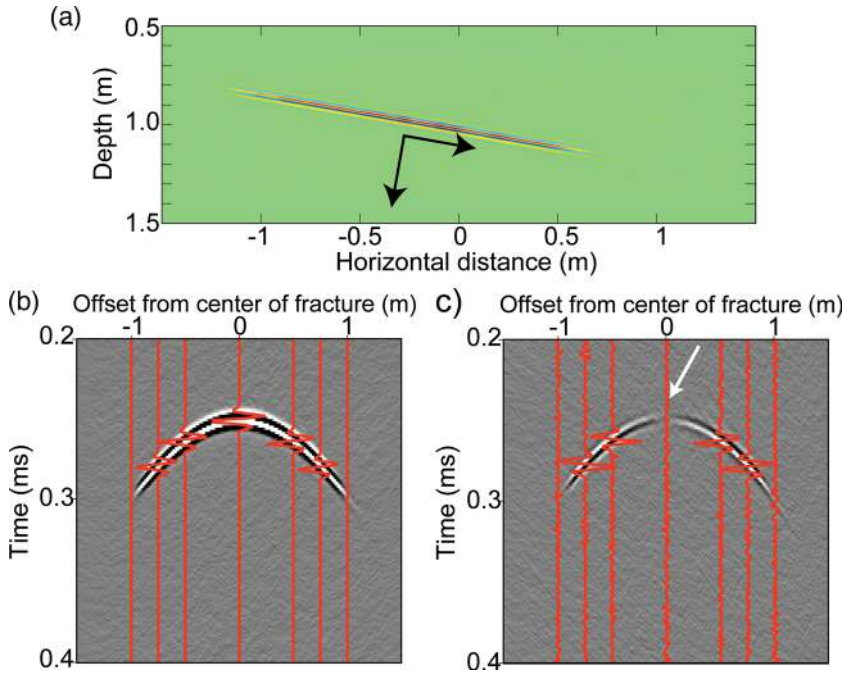

Figure 3. (a) Result of reverse time migration. The black arrows show the fracture-oriented axes. (b) Extrapolated scattered wavefield (vertical component of the particle velocity) along the fracture. The axes are already rotated so that the horizontal axis aligns along the fracture plane [see arrow in (a)]. The red traces show the waveforms. (c) Same as (b) but for the horizontal component of the particle velocity in the rotated axis.

Next we image the unknown position and dip of the fracture. For this purpose, we use reverse-time migration (e.g. Chang & McMechan 1994; Yan & Sava 2008). The migration uses the eqs (1) and (2) for wavefield extrapolation followed by application of the imaging condition, for which we use the zero-lag cross-correlation amplitude (Yan & Sava 2008). Fig. 3(a) shows the migrated image from the *P*–*P* reflections. Note that this image is obtained using only one source. One can use multiple source responses to increase the signal-to-noise ratio. The fracture position and the dip are estimated by using the picked maximum amplitude of the migrated image followed by a linear least-square fitting. This leads to an accurate estimation of the fracture position and dip (the estimated dip is 9.99°). The black arrows in Fig. 3(a) show the fracture-oriented axes extracted from the migrated image. In this context, the use of the converted *S* wave in migration will also be beneficial in the VSP configuration (Nihei *et al.* 2000).

Figs 3(b) and (c) show the extrapolated backscattered wavefield (particle velocity) along the imaged fracture position. The axes are already rotated so that the horizontal axis lies in the fracture plane (arrow in Fig. 3a). Because the scattered response is back-propagated (eq. 2), the traveltime of the strong events is earlier than those of the input data (Fig. 2). Furthermore, because *P* and converted-*S* waves are originated at the same position (fracture plane), these two wavefields are back-propagated and they appear at the same traveltime. Due to the applied noise, the low-amplitude diffracted (coda) waves are contaminated with high noise. However, the strong specular reflections are correctly extrapolated. Red traces in Figs 3(b) and (c) show the waveforms of the extrapolated wavefield. The horizontal particle velocity along the new (rotated) axis (Fig. 3c) shows almost zero amplitude at the centre of the fracture (see the white arrow in Fig. 3c). This shows that because of the normal *P*-wave incidence, there is no converted *S* wave at this position of the fracture. The same result can also be obtained from *P*-to-*SV* reflection coefficients (Schoenberg 1980; Chaisri & Krebes 2000). As we will see in the next section, this is responsible for the loss in quality of the tangential compliance estimated from *P*-wave point source response through the inverse scattering solution.

Once the stress field along the fracture plane is estimated, one can estimate the heterogeneous compliance distribution. It solves the boundary condition represented in the frequency–wavenumber domain as,

$$\hat{\mathbf{A}}(k_x) = \mathrm{i}\omega\hat{\mathbf{Z}}(k_x) * \hat{\mathbf{B}}(k_x), \tag{3}$$

where the functions $\hat{\mathbf{A}}$ and $\hat{\mathbf{B}}$ are calculated from the stress field at the fracture as,

$$\hat{\mathbf{A}} = \hat{\mathbf{H}}\hat{\tau}^{-}, \tag{4}$$

$$\hat{\mathbf{B}} = \hat{\tau}^{-} + \hat{\tau}^{+}, \tag{5}$$

$$\hat{\mathbf{H}} = \hat{\mathbf{L}}_1^{+}(\hat{\mathbf{L}}_2^{+})^{-1} - \hat{\mathbf{L}}_1^{-}(\hat{\mathbf{L}}_2^{-})^{-1}. \tag{6}$$

Eqs (4)–(6) require that there is no upgoing wave in the lower medium (Minato & Ghose 2013). Furthermore, $\hat{\mathbf{L}}_1^{\pm}$ includes elastic constants of the medium. After inverse Fourier transformation of eq. (3), we obtain the heterogeneous compliance distributions as,

$$\eta_T(x) = \frac{\mathbf{A}(x)\cdot\mathbf{e}_1}{\mathrm{i}\omega(1+\epsilon^{\mathrm{reg}}/r_T)\mathbf{B}(x)\cdot\mathbf{e}_1}, \tag{7}$$

$$\eta_N(x) = \frac{\mathbf{A}(x)\cdot\mathbf{e}_2}{\mathrm{i}\omega(1+\epsilon^{\mathrm{reg}}/r_N)\mathbf{B}(x)\cdot\mathbf{e}_2}, \tag{8}$$

$$r_T = |\mathbf{B}(x)\cdot\mathbf{e}_1| \tag{9}$$

$$r_N = |\mathbf{B}(x)\cdot\mathbf{e}_2|, \tag{10}$$

where $\mathbf{e}_i$ is a unit vector, that is, $\mathbf{e}_1 = (1\ 0)^T$ and $\mathbf{e}_2 = (0\ 1)^T$. ϵ^{reg} denotes a regularization factor to stabilize the solution.

Fig. 4(a) shows the estimated normal compliance distribution using eq. (8) with $\epsilon^{\mathrm{reg}} = 1E-12$. Since eq. (8) is formulated in

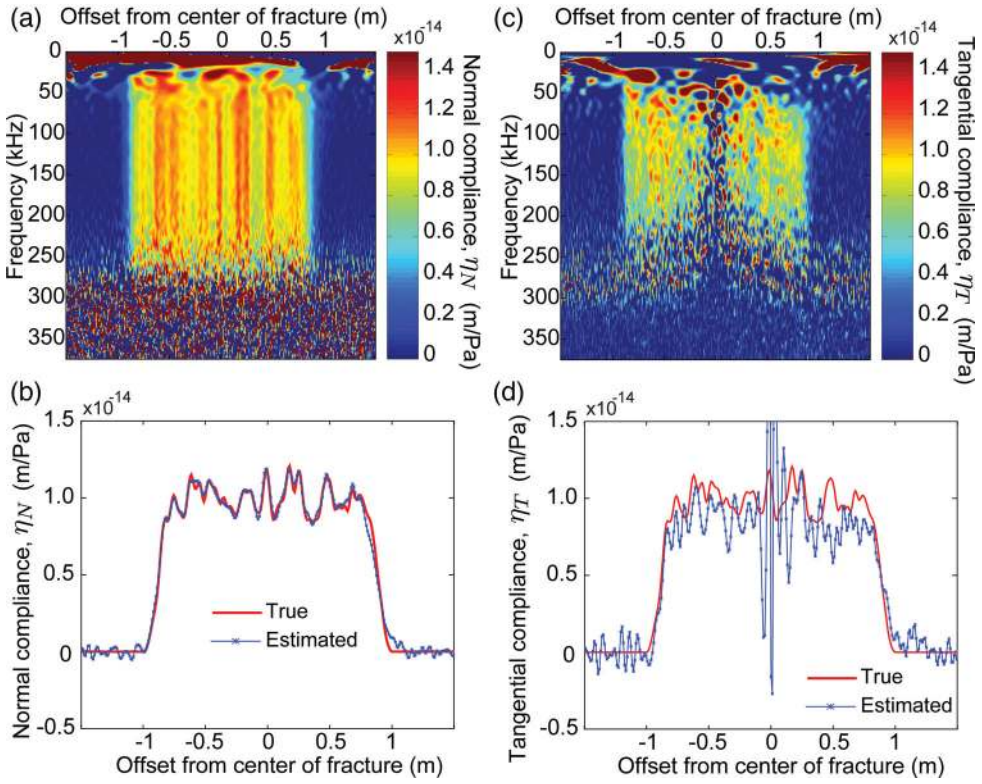

Figure 4. (a) Estimated normal fracture compliance using inverse scattering solution of a *P*-wave point source response. (b) Comparison of the estimated normal compliance distribution at the dominant frequency (100 kHz) with the true compliance distribution. (c) Same as (a) but for the tangential fracture compliance. (d) Same as (b) but for the tangential fracture compliance.

the frequency-space domain, we can estimate the heterogeneous compliance distribution at each frequency (Fig. 4a). The estimated compliance distribution around the dominant frequency of the incident wavefield (100 kHz) is very accurate (Fig. 4b). The higher frequency components (>250 kHz) are noisy due to the white noise. At frequencies below 50 kHz, the estimated compliance is smooth and inaccurate. This is mainly because of the presence of the evanescent waves, which are not correctly back-propagated by our matched operator (eq. 2). The evanescent waves dominate at low frequencies (Minato & Ghose 2013). The effect of the presence of evanescent waves, the receiver spacing and the varying noise level in the data has been studied in detail in Minato & Ghose (2013). The successful application of this method relies on the accuracy of the wavefield extrapolation in depth. Therefore, the experiment needs to be designed so as to allow extrapolation of the wavefield with sufficient accuracy. The method requires an accurate estimation of the extrapolation velocity. Large errors in the velocity will distort the migration image, which will cause errors in fracture location. In this case, the estimated compliance will have imaginary components (Minato & Ghose 2013).

Fig. 4(c) shows the estimated tangential compliance distribution using eq. (7). As pointed out by Chaisri & Krebes (2000), *P–P* and *P–SV* reflection coefficients are always more sensitive to the normal compliance than the tangential compliance, considering the maximum incidence angle in our experiment to be about 56°. Furthermore, around the normal incidence, the sensitivity of the converted *S* wave to the tangential compliance is larger than that of the reflected *P* wave (Chaisri & Krebes 2000). As shown in the previous section, the converted *S* wave is nearly absent around the normal incidence as we have considered only a *P*-wave source. This explains why we require a larger stabilization factor ($\epsilon^{\text{reg}} = 1.5E - 10$) to estimate the tangential compliance than for the normal compliance. The estimated tangential compliance (Fig. 4c) is less accurate than the normal compliance (Fig. 4b), especially around the centre of the fracture (see Fig. 4d for dominant frequency). In this case, the use of multiple sources will certainly be useful as that will increase the number of grazing angles to avoid the shadow zone for the tangential compliance. Use of an *S*-wave source is also expected to increase the accuracy of the tangential compliance.

4 CONCLUSION

The inverse scattering of elastic waves is useful to obtain realistic values of the spatial distribution of fracture compliances, for example, the magnitude of the variation and its spatial correlation along the fracture surface. We have demonstrated in this paper that the inverse scattering solution can be applied to a seismic point source response of a homogeneous medium containing a subhorizontal fracture. This is a realistic evaluation for the situation where the seismic source is located close to the fracture and the receivers, in the scale of the seismic wavelength. Also, with only a *P*-wave point source response, it is possible to estimate both normal and tangential fracture compliances. In order to apply the method to dipping fractures, one needs to extract the wavefield along the inclined fracture plane followed by axes rotation. For this purpose, the knowledge of the fracture position and dip is necessary. This can be achieved through reverse-time migration.

We have calculated the wavefield from a *P*-wave point source in a 2-D elastic medium using FDTD method. We compare the scattered wavefield between homogeneous and heterogeneous fracture compliance distributions. Significantly, we find the differences to

be conspicuous in the amplitude of the specular reflections and in the presence of the non-specular diffracted energy. We have applied reverse-time migration to the *P*–*P* reflections to estimate the position of the fracture and its orientation. The maximum amplitude in the migrated image has been picked, followed by a least-square linear fitting. This has offered accurate estimates of fracture position and fracture dip. In order to solve the inverse scattering problem, we have performed forward extrapolation of the incident wavefield and backward extrapolation of the scattered wavefield. The extracted wavefield along the identified fracture position is then rotated so that the horizontal axis aligns in the fracture plane. The extracted and rotated wavefield shows that, for a *P*-wave point source, there is no converted *S* wave at the normal incidence, which is expected. Next, using these extracted wavefields, we solved the displacement–discontinuity boundary condition to estimate normal and tangential compliance distributions in space. The normal compliance is accurately estimated at the dominant seismic frequency. At low frequencies, however, the estimated compliance distribution is smooth and less accurate. This is due to the prevalence of the evanescent waves at low frequencies. The estimation of the tangential compliance distribution requires a larger stabilization factor; the estimate is less accurate than that of the normal compliance distribution. This is mainly because of the use of only a *P*-wave point source and the absence of the converted *S* wave at normal incidence. For an accurate estimation of the tangential compliance, one may use *S*-wave sources instead of *P*-wave sources and/or multiple sources which increases the number of grazing angles to avoid the shadow zone for the tangential compliance. Note that in our illustration, we have estimated the compliance using a single common-source gather. The presence of multiple sources, as is usual in field measurements, will increase the accuracy of the estimated compliance.

ACKNOWLEDGEMENTS

This work is supported by The Netherlands Research Centre for Integrated Solid Earth Science (ISES).

REFERENCES

Acosta-Colon, A., Pyrak-Nolte, L.J. & Nolte, D.D., 2009. Laboratory-scale study of field of view and the seismic interpretation of fracture specific stiffness, *Geophys. Prospect.,* **57**(2), 209–224.

Baik, J.-M. & Thompson, R.B., 1984. Ultrasonic scattering from imperfect interfaces: a quasi-static model, *J. Nondestruct. Eval.,* **4**(3-4), 177–196.

Baird, A.F., Kendall, J.M. & Angus, D.A., 2013. Frequency-dependent seismic anisotropy due to fractures: fluid flow versus scattering, *Geophysics,* **78**(2), WA111–WA122.

Biwa, S., Hiraiwa, S. & Matsumoto, E., 2007. Stiffness evaluation of contacting surfaces by bulk and interface waves, *Ultrasonics,* **47,** 123–129.

Chaisri, S. & Krebes, E.S., 2000. Exact and approximate formulas for P-SV reflection and transmission coefficients for a nonwelded contact interface, *J. geophys.Res.: Solid Earth,* **105**(B12), 28 045–28 054.

Chang, W. & McMechan, G., 1994. 3-D elastic prestack, reverse-time depth migration, *Geophysics,* **59**(4), 597–609.

Coates, R. & Schoenberg, M., 1995. Finite difference modeling of faults and fractures, *Geophysics,* **60**(5), 1514–1526.

Hudson, J.A., Liu, E. & Crampin, S., 1997. The mean transmission properties of a fault with imperfect facial contact, *Geophys. J. Int.,* **129**(3), 720–726.

Leiderman, R., Barbone, P.E. & Braga, A.M.B., 2007. Reconstructing the adhesion stiffness distribution in a laminated elastic plate: exact and approximate inverse scattering solutions, *J acoust. Soc. Am.,* **122**(4), 1906–1916.

Lubbe, R., Sothcott, J., Worthington, M. & McCann, C., 2008. Laboratory estimates of normal and shear fracture compliance, *Geophys. Prospect.,* **56**(2), 239–247.

Minato, S. & Ghose, R., 2013 Inverse scattering solution for the spatially heterogeneous compliance of a single fracture, *Geophys. J. Int.,* **195,** 1878–1891.

Minato, S. & Ghose, R., 2014. Power spectral density of the heterogeneous fracture compliance from the scattered elastic wavefield, *Geophysics,* **79**(2), doi:10.1190/GEO2013-0173.1.

Nihei, K., Nakagawa, S. & Myer, L., 2000. VSP fracture imaging with elastic reverse time migration, *SEG Tech. Prog. Expanded Abstracts,* **445,** 1748–1751.

Oliger, A., Nolte, D.D. & Pyrak-Nolte, L.J., 2003. Seismic focusing by a single planar fracture, *Geophys. Res. Lett.,* **30**(5), 1203.

Pyrak-Nolte, L. & Nolte, D., 1992. Frequency dependence of fracture stiffness, *Geophys. Res. Lett,* **19**(3), 325–328.

Sayers, Colin M., 2002. Fluid-dependent shear-wave splitting in fractured media, *Geophys. Prospect.,* **50**(4), 393–401.

Schoenberg, M., 1980. Elastic wave behavior across linear slip interfaces, *J. acoust. Soc. Am.,* **68**(5), 1516–1521.

Wapenaar, C. & Berkhout, A., 1989. *Elastic Wave Field Extrapolation: Redatuming of Single-and Multi-Component Seismic Data,* Elsevier Science.

Willis, M., Burns, D., Rao, R., Minsley, B., Toksöz, M. & Vetri, L., 2006. Spatial orientation and distribution of reservoir fractures from scattered seismic energy, *Geophysics,* **71**(5), O43–O51.

Worthington, M.H. & Hudson, J.A., 2000. Fault properties from seismic Q, *Geophys J. Int.,* **143**(3), 937–944.

Worthington, M.H. & Lubbe, R., 2007. The scaling of fracture compliance, *Geol. Soc., Lond., Spec. Publ.,* **270**(1), 73–82.

Yan, J. & Sava, P., 2008. Isotropic angle-domain elastic reverse-time migration, *Geophysics,* **73**(6), S229–S239.